# Electrical determination of vortex state in submicron magnetic elements

Ajay Gangwar,[1,2] Hans G. Bauer,[1] Jean-Yves Chauleau,[1] Matthias Noske,[2] Markus Weigand,[2] Hermann Stoll,[2] Gisela Schütz,[2] and Christian H. Back[1]

[1]*Department of Physics, University of Regensburg, Universitätsstraße 31, 93040 Regensburg, Germany*

[2]*Max Planck Institute for Intelligent Systems, Heisenbergstraße 3, 70569 Stuttgart, Germany*

(Received 16 January 2015; revised manuscript received 23 February 2015; published 10 March 2015)

We have studied vortex dynamics excited by the spin-transfer-torque effect and find that the direction of the vortex state can be detected electrically using the homodyne voltage signal generated due to the anisotropic magnetoresistance (AMR) effect. An external in-plane dc magnetic field is required to break the cylindrical symmetry in order to obtain a dc response of the homodyne signal. The sign of this rectified voltage changes with the handedness of the vortex state, which makes it a promising method to detect the vortex state electrically. Vortex dynamics is also observed by direct imaging in a scanning transmission x-ray microscope, allowing verification of the measured AMR signal in the correct power and frequency range. The results of micromagnetic simulations are in good agreement with the experimental data.

DOI: 10.1103/PhysRevB.91.094407 PACS number(s): 75.78.Fg, 75.78.Cd, 85.70.−w

Vortex structures [1,2] in confined geometries are currently under close scrutiny due to their unique properties associated with their spatial confinement and the nonuniform distribution of the magnetization. The magnetic vortex is characterized by two Boolean topological quantities: chirality (clockwise or counterclockwise orientation, $c = \pm 1$) of the in-plane magnetization and polarity (up or down, $p = \pm 1$) of the vortex core (VC) (diameter 10–20 nm) [2,3]. As a result, there are four different energetically equivalent ground states which are more stable than conventional magnetic domains and can accelerate the development of compact and high performance spin-transfer torque oscillators for rf generation on the nanoscale as well as magnetic memory devices [4], if they can be harnessed and manipulated. Thus, an understanding of the dynamic behavior of elements in the vortex state, their control, as well as a way to electrically detect the vortex state ($c$ and $p$) is a major requirement for their further development and for successful implementation in magnetic data storage devices. Progress can be achieved by combining theoretical calculations, micromagnetic simulations, and experimental approaches.

In the last decade much work has been dedicated to manipulating the vortex state [5–18]. Vortex dynamics can be excited and the VC's polarity can be controlled by an in-plane oscillating magnetic field or by passing an rf current through the magnetic element. Vortex structures are investigated by several methods, e.g., magnetic force microscopy (MFM) [1,2], magneto-optical Kerr effect (MOKE) [6], and scanning transmission x-ray microscopy (STXM) [15–18], however, these methods cannot be implemented in technological applications. Here we present a set of measurements combined with micromagnetic simulations on micron sized magnetic elements exhibiting a vortex state, allowing us to detect complete information of the vortex state ($c$ and $p$) electrically. The technique used is based on the rectification of a periodic homodyne voltage signal due to a periodic change in resistance of the magnetic element as a function of the position of the vortex core. We follow the excitation of the VC from the linear to the nonlinear regime in a square where the VC is attached to the domain walls in a Landau domain structure and in a disk, and support our findings with micromagnetic simulations.

Vortex core dynamics [19] can be excited with the spin-transfer-torque (STT) effect [20] by flowing an alternating current through the magnetic element. The time evolution of the magnetization $\vec{M}$ is given by the extended Landau-Lifshitz-Gilbert (LLG) equation [21,22] including STT terms [23,24],

$$\dot{\vec{m}} = -|\gamma|\vec{m} \times \vec{H}_{\text{eff}} + \alpha\vec{m} \times \dot{\vec{m}} - (\vec{u} \cdot \vec{\nabla})\vec{m} + \beta\vec{m} \times [(\vec{u} \cdot \vec{\nabla})\vec{m}]. \quad (1)$$

Here $\vec{m}$ is a unit vector in the direction of $\vec{M}$ and $\vec{u}$ is a vector directed along the direction of electron motion of magnitude $u = jPg\mu_B/2eM_s$, with current density $j$, polarization $P$ of the conduction electrons, $e$ the electron charge, $g$ the $g$ factor, $\mu_B$ the Bohr magneton, and $M_s$ the saturation magnetization. The first term corresponds to the precession of the magnetization around the effective field $\vec{H}_{\text{eff}}$. This term conserves the angle between $\vec{M}$ and $\vec{H}_{\text{eff}}$ and thus conserves the energy of the system. The precession rate is proportional to $\vec{H}_{\text{eff}}$ with a proportionality factor $\gamma$, the gyromagnetic ratio. The second term in this equation represents the damping torque. The damping parameter $\alpha$ determines how fast the magnetization relaxes towards the direction of the effective magnetic field. The last two terms represent the dynamics due to STT induced by a current density $\vec{j}$ flowing through it, where $\beta$ is the nonadiabatic parameter. We note that this equation is nonlinear and thus one may expect complicated dynamics in some range of adjustable parameters. Furthermore, the dynamics in special cases of magnetic textures, e.g., vortex structures, can be described by modifying the LLG equation to the Thiele equation [19,24,25],

$$\vec{F} + \vec{G} \times (\vec{v} - \vec{u}) + D(\alpha\vec{v} - \beta\vec{u}) = 0. \quad (2)$$

This is the force balance equation originally reported by Thiele [25] to describe the dynamic properties of magnetic domain walls. $\vec{F}$ is the force from the effective field $\vec{H}_{\text{eff}}$ originally appearing in the LLG equation and the gyrotropic vector $\vec{G}$ is perpendicular to the film plane given by $\vec{G} = (2\pi pqLM_s/\gamma)\hat{z}$

 

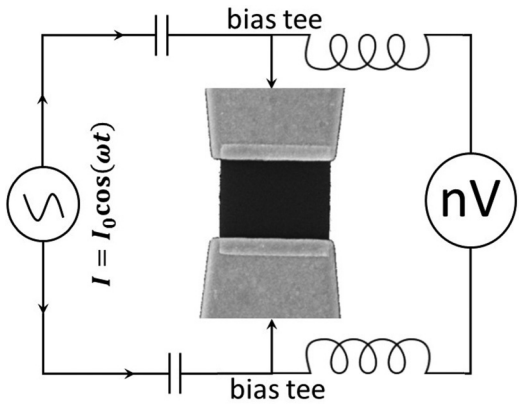


FIG. 1. Schematic illustration of the experimental setup.

if we put the film in the $(x,y)$ plane. Here, $L$ is the thickness, the topological charge $q = \pm 1, \pm 2, \ldots$ is the vorticity, and $p$ is the vortex core polarity. Thus the second term in this equation determines the sense of gyration of the vortex core. The total dissipation force is given by the third term with the dissipation tensor $\vec{D}$ and the vortex core velocity $\vec{v}$.

The measurements are performed on a Permalloy square with an edge length of 1.6 $\mu$m and a thickness of 50 nm, as well as on a disk with the same thickness and a diameter of 1.6 $\mu$m. The devices are prepared by a combination of optical and electron beam lithography and lift-off process. To perform STXM measurements, the magnetic elements are placed on a 100 nm thin SiN membrane to facilitate the transmission of x rays. Two Au contacts are attached on opposite edges of the samples to excite vortex dynamics by passing a current through them. The voltage drop across the sample is measured using a nanovoltmeter via a bias tee, as sketched in Fig. 1.

To identify the resonance frequency of the vortex gyrotropic mode in the samples, we first observe vortex core dynamics directly in a scanning transmission x-ray microscope at the MAXYMUS endstation at BESSY II, Berlin, with high temporal (less than 100 ps) and spatial (25–30 nm) resolution. The x-ray magnetic circular dichroism (XMCD) effect [26] allows one to detect the out-of-plane magnetic contrast of the core when the sample is placed perpendicular to the photon beam direction. The measurements are performed at the Ni $L_3$ absorption edge (852.7 eV). The gyrotropic motion of the VC is driven with an rf current and the frequency is tuned near the expected resonance frequency of the magnetic element [27]. When the frequency reaches resonance, the radius of gyration ($r$) exhibits a maximum. The radius of gyration of the VC as a function of excitation frequency is plotted in Fig. 2(a). The resonance curve yields a resonant frequency of about 205 MHz, which is in very good agreement with that determined by micromagnetic simulations.

Next we measure the anisotropic magnetoresistance (AMR) of the elements as a function of excitation frequency ($f = \omega/2\pi$) in the vicinity of the resonance frequency of the VC. Due to the AMR effect, the resistance of the ferromagnetic elements depends upon the relative orientation of the magnetization with respect to the current flow direction [28]. When an rf current $I = I_0 \cos(\omega t)$ flows through the element exhibiting a vortex structure, STT causes the VC to gyrate around its

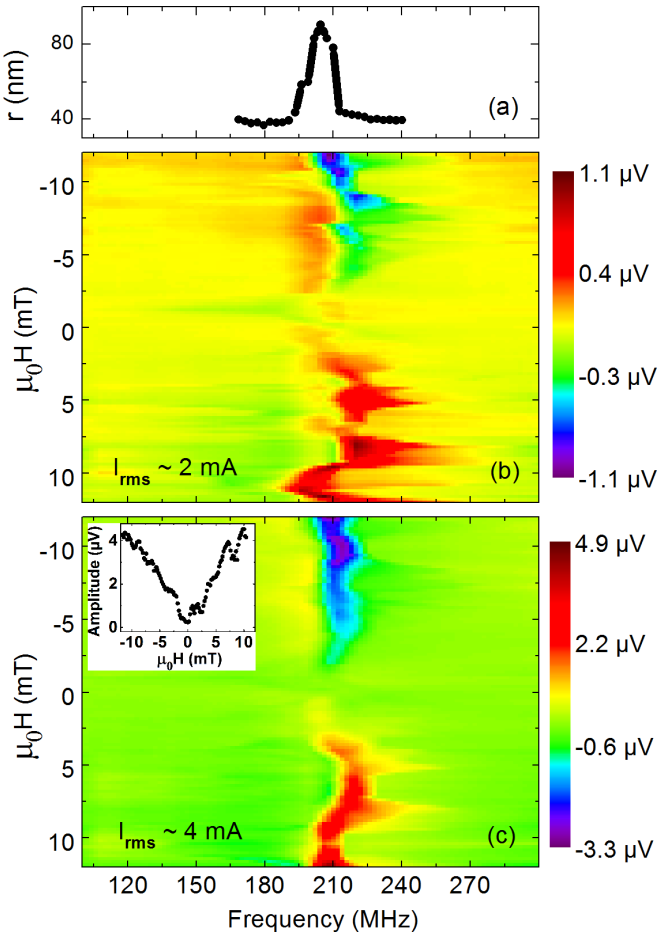


FIG. 2. (Color online) (a) Resonance curve for the gyroradius ($r$) of the vortex core, measured by real time imaging of the vortex dynamics directly in the STXM. (b) AMR spectra measured on a square shaped sample for two different excitation currents [2 mA in (b) and 4 mA in (c)]. The inset in (c) shows the amplitude of the AMR signal at 4 mA, as a function of bias field.

equilibrium position. The gyrotropic motion leads to a periodic change of the magnetic structure and hence its resistance [$R = \Delta R \cos(2\omega t + \phi)$] changes with twice the frequency of the rf current, where $\phi$ is the phase between excitation and motion of the vortex core. The current flowing through the sample mixed with the change in resistance produces a homodyne voltage signal [29] which can be understood simply following Ohm's law,

$$V = IR = V_0[\cos(\omega t + \phi) + \cos(3\omega t + \phi)]. \quad (3)$$

This homodyne signal can be measured, e.g., in an oscilloscope, and vortex dynamics can be investigated. However, we are interested in rectifying the signal and in measuring a dc response of this homodyne voltage signal. We therefore use an external dc magnetic field to break the symmetry of the magnetic configuration, and then the resistance and the resulting homodyne voltage signal can be expressed as

$$R = \Delta R \sum_{n \neq 0} A_n \cos(n\omega t + \phi), \quad (4)$$

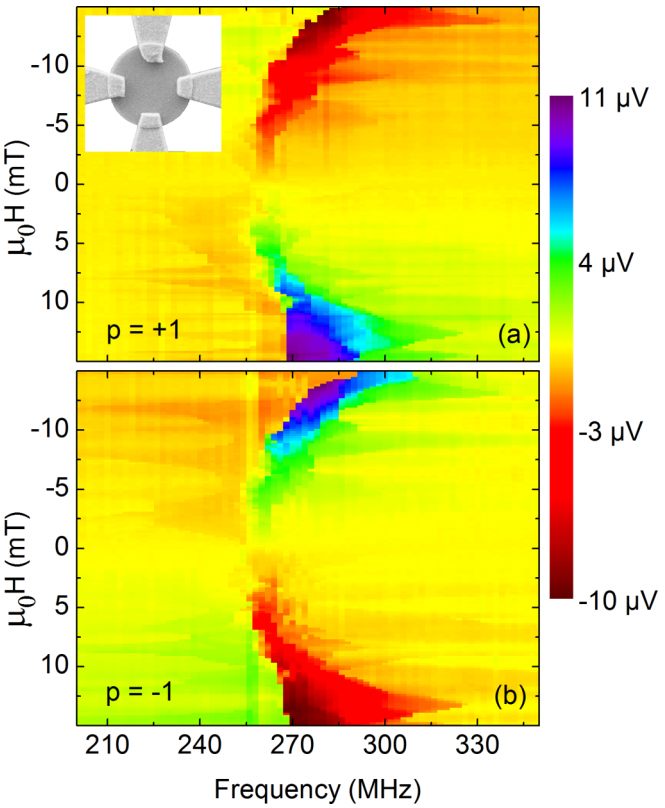


FIG. 3. (Color online) AMR spectra measured on a disk shaped sample for (a) up ($p = +1$) and (b) down ($p = -1$) polarization of the vortex core for an excitation current of 1.2 mA. The sample design is shown in the inset of (a). By applying a rotating current (counterclockwise or clockwise) the VC polarity can be switched selectively to up or down. A sign change of the AMR voltage signal can be observed for the two polarities. Note that a significant shift of the resonance frequency to higher frequencies is observed at larger bias fields. Also note that the fine structure observed in the spectra does not depend on the VC polarity.

$$V = V_0 \left[ B_1 \cos(\phi) + \sum_{n \neq 0} B_n \cos(n\omega t + \phi) \right], \qquad (5)$$

$$V = V_{\mathrm{dc}} + V_{\mathrm{ac}}. \qquad (6)$$

This means that the resistance change has a component at the excitation frequency which mixes with the rf current and generates a dc voltage signal to be measured in a nanovoltmeter. The normalized AMR spectra shown in Figs. 2(b), 2(c), and 3 are obtained by subtracting the signal at zero external applied dc field since there is no dc component for zero external field, as discussed above. Figures 2(b) and 2(c) show the measured rectified resonance spectra of the AMR signal generated from the gyrotropic motion of the VC as a function of bias fields for two different excitation currents [2 mA in Fig. 2(b) and 4 mA in Fig. 2(c)] for the square shaped element. We observe that a large AMR signal appears near 205 MHz which corresponds to the resonance frequency of the element as measured in STXM [see Fig. 2(a)]. With increasing external field the asymmetry of the Landau domain structure increases and hence the amplitude

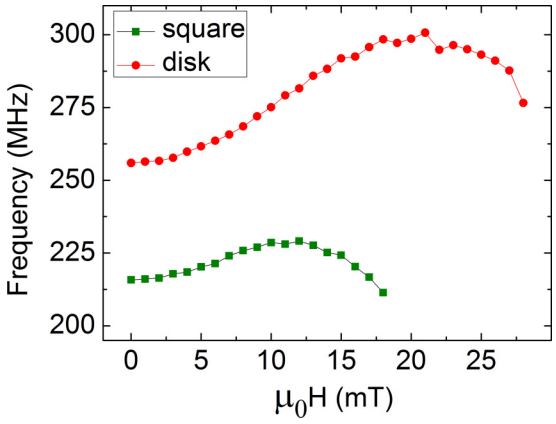


FIG. 4. (Color online) Micromagnetic simulations for the resonance frequency as a function of bias fields. The resonance frequency shows a larger shift to higher frequencies for the disk shaped sample in comparison to the square shaped sample, in good agreement with the experiments. To expel the vortex core from the sample, a higher external field is required for the disk.

of the AMR signal also increases, as shown in the inset of Fig. 2(c). We further observe that with increasing external magnetic field the position of the resonance remains almost constant. The observed deviations of the resonance peak position as a function of bias field can be attributed to local modifications of the magnetic properties of the sample, since the gyrating vortex core is scanned across the sample when applying the external magnetic field [30]. With increasing power [Fig. 2(c)], the gyroradius increases, and the effect of random local deviations thus averages out on the longer gyrotrajectory. Note that the gyrating VC can be effectively used to investigate the magnetic inhomogeneity of the samples [30]. In fact, in Figs. 3(a) and 3(b) we show that the observed fine structure is unchanged when the VC polarity is reversed.

In order to be able to investigate the AMR signal for the two polarities of the vortex core, a disk shaped sample of diameter 1.6 $\mu$m and thickness 50 nm with four contacts is used. In this configuration, the VC polarity can be switched selectively [15,16] to the up (down) state by a counterclockwise (clockwise) rotating current. The direction of the core gyration is solely determined by the VC polarity. The VC with up ($p = +1$) polarity rotates in the counterclockwise direction and the VC with down ($p = -1$) polarity in the clockwise direction. Therefore, a phase difference of 180° occurs between the dynamics of the VC with the two opposite polarities, which results in a sign change of the homodyne voltage signal. Figure 3 clearly shows a sign reversal in the AMR spectra for two polarities of the vortex core. Also, we now notice a significant shift in the resonance frequency with bias field which is not so pronounced in the case of the square shaped element. This indicates that the magnetization in the disk shaped sample is becoming stiffer with increasing external field, which results in an increase of the resonance frequency. Our micromagnetic simulations confirm such an initial increase in the resonance frequency and a later decrease (see Fig. 4). We attribute the decrease, i.e., a softening of the gyro mode, to the single vortex state becoming unstable [27]

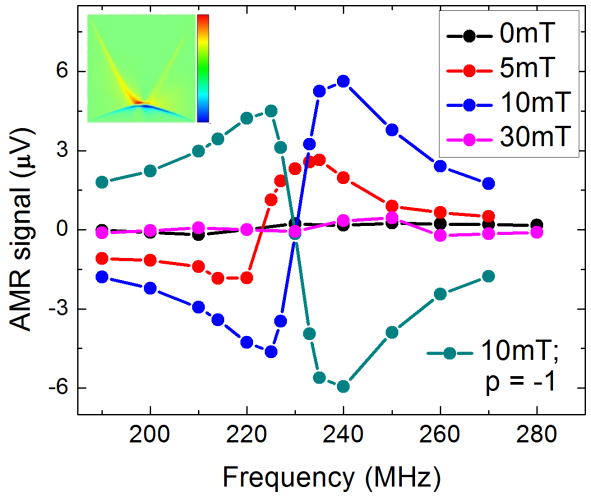


FIG. 5. (Color online) Micromagnetic simulations of the rectified AMR signal for various bias fields obtained on the square shaped sample. The sign of the AMR signal changes when the vortex polarity is reversed, as shown for the case of 10 mT, where both cases $p = +1$ and $p = -1$ are shown. We do not observe any AMR signal for zero magnetic field due to symmetry reasons and for fields (30 mT) large enough to expel the VC from the sample. The inset shows the spatial contribution to rectified AMR signal.

and the initial increase to the extra energy that is connected with a domain-wall-like distortion of the magnetization that starts to form with increasing external field.

To compare and verify the experimental results, micromagnetic simulations are performed with MUMAX [31] for a square of edge length 1.6 $\mu$m and thickness 50 nm with material parameters chosen to mimic Permalloy as follows: saturation magnetization $(M_s) = 800 \times 10^3$ A/m, damping constant $(\alpha) = 0.006$, and exchange parameter $A = 1.3 \times 10^{-11}$ J/m. As the vortex core diameter is about 10 nm, a cell size of 3.125 nm is chosen. Figure 5 shows simulated resonant curves for the AMR signal for different bias fields which show a large signal near a frequency of 205 MHz. For 0 mT external field there is no resonance line, as expected and explained earlier. For external biases of 5 and 10 mT we find a resonance line with resonance frequency near 205 MHz. For a bias field of 30 mT, the magnetic element is no longer in the vortex state and therefore no AMR signal is observed. The sign of the rectified AMR signal depends upon the polarity of the vortex core, as shown for the case of $p = \pm 1$ at 10 mT bias field. Additionally, spatially resolved contributions to the rectified AMR signal for a bias field of 15 mT, an rf current of 10 mA amplitude, and 210 MHz frequency are shown in the inset of Fig. 5. Here we notice that the main contribution is concentrated in the lines (domain walls) connecting the vortex core with the four corners of the square, and the magnitude of the AMR signal (sum over the whole square) depends upon the position of the vortex core. The reason for the signal occurring in these regions is that here the magnetization changes periodically, which leads to a periodic change in resistance of the sample. If the polarity of the vortex core is reversed, the positive (red) and negative (blue) contributions exchange sign and thus the effective dc response will also change sign, which also explains the change of sign with polarity. In the absence of a bias field, the VC will be at the center of the square, and in this case the positive (red) and negative (blue) contributions are equal and will cancel each other, which will result in no AMR signal for zero bias. If we change the chirality of the vortex structure or the direction of the bias field, the vortex core will be at the opposite sides of the square, which will increase (decrease) the positive (negative) contribution or, in other words, the sign of the AMR signal will be reversed again with a change of bias field direction (or chirality), as shown in the measured spectra for positive and negative fields (Figs. 2 and 3).

The experimental and simulation results show that the sign of the AMR signal depends upon the handedness ($cp$) of the vortex structure. Thus two out of the four possible configurations ($c$ and $p$) of the vortex state will generate a positive AMR signal and the other two will generate a negative signal for the same excitation parameter and bias field. To distinguish all four states independently, we can utilize in-plane exchange biased vortex structures [32,33]. Micromagnetic simulations carried out by Heinonen *et al.* [33] have shown that the resonance frequency of the vortex core increases with the magnitude of the exchange bias, considering that the exchange bias field follows the direction of the magnetization in the ferromagnetic layer. We have performed a similar micromagnetic simulation [34] and found that if we keep the direction of exchange bias and change the chirality of the vortex structure, there is a splitting of the resonance frequencies for the two chiralities of the vortex state, irrespective of the polarity. When the exchange bias field follows the magnetization of the vortex structure, the resonance frequency is higher (202 MHz) and it is lower (119 MHz) for the other chirality compared to the one in the absence of exchange bias (161 MHz). Thus, by exploiting the exchange bias in vortex structures, we expect to obtain positive and negative AMR signals for two polarities of the vortex core at a higher frequency in the case of one chirality and similar signals at a lower frequency for the other chirality. We note that the circulation can be switched selectively by application of a magnetic field when slight asymmetries in the shape of the vortex state elements are introduced [10,13].

In conclusion, we have observed vortex dynamics by analyzing the rectified homodyne AMR signal, and we are able to determine the vortex state electrically. The experimental results are consistent with micromagnetic simulations, which give us a better understanding of the origin of the voltage signal and support the validity of our technique. The distribution of local modifications of the magnetic properties across the magnetic element can be characterized by analyzing the measured resonant curves for different directions and strengths of the external bias field. Our detailed simulations and experimental analysis show that both chirality and polarity of the vortex state can be detected electrically and may help to implement vortex structures in future nonvolatile magnetic data storage devices.

The work has been partially funded by the Deutsche Forschungsgemeinschaft via SFB 689. J.Y.C. would like to acknowledge support from the AvH foundation.

[1] J. Raabe, R. Pulwey, R. Sattler, T. Schweinbck, J. Zweck, and D. Weiss, J. Appl. Phys. **88**, 4437 (2000).

[2] T. Shinjo, T. Okuno, R. Hassdorf, K. Shigeto, and T. Ono, Science **289**, 930 (2000).

[3] J. Miltat and A. Thiaville, Science **298**, 555 (2002).

[4] S. Bohlens, B. Krger, A. Drews, M. Bolte, G. Meier, and D. Pfannkuche, Appl. Phys. Lett. **93**, 142508 (2008).

[5] S.-B. Choe, Y. Acremann, A. Scholl, A. Bauer, A. Doran, J. Stöhr, and H. A. Padmore, Science **304**, 420 (2004).

[6] J. P. Park and P. A. Crowell, Phys. Rev. Lett. **95**, 167201 (2005).

[7] V. Novosad, F. Y. Fradin, P. E. Roy, K. S. Buchanan, K. Y. Guslienko, and S. D. Bader, Phys. Rev. B **72**, 024455 (2005).

[8] B. Van Waeyenberge, A. Puzic, H. Stoll, K. W. Chou, T. Tyliszczak, R. Hertel, M. Fähnle, H. Bruckl, K. Rott, G. Reiss, I. Neudecker, D. Weiss, C. H. Back, and G. Schütz, Nature (London) **444**, 461 (2006).

[9] K. Yamada, S. Kasai, Y. Nakatani, K. Kobayashi, H. Kohno, A. Thiaville, and T. Ono, Nat. Mater. **6**, 270 (2007).

[10] T. Kimura, Y. Otani, H. Masaki, T. Ishida, R. Antos, and J. Shibata, Appl. Phys. Lett. **90**, 132501 (2007).

[11] G. de Loubens, A. Riegler, B. Pigeau, F. Lochner, F. Boust, K. Y. Guslienko, H. Hurdequint, L. W. Molenkamp, G. Schmidt, A. N. Slavin, V. S. Tiberkevich, N. Vukadinovic, and O. Klein, Phys. Rev. Lett. **102**, 177602 (2009).

[12] F. G. Aliev, J. F. Sierra, A. A. Awad, G. N. Kakazei, D.-S. Han, S.-K. Kim, V. Metlushko, B. Ilic, and K. Y. Guslienko, Phys. Rev. B **79**, 174433 (2009).

[13] V. Uhlir, M. Urbanek, L. Hladik, J. Spousta, M.-Y. Im, P. Fischer, N. Eibagi, J. J. Kan, E. E. Fullerton, and T. Sikola, Nat. Nanotechnol. **8**, 341 (2013).

[14] R. Hertel, S. Gliga, M. Fähnle, and C. M. Schneider, Phys. Rev. Lett. **98**, 117201 (2007).

[15] M. Curcic, B. Van Waeyenberge, A. Vansteenkiste, M. Weigand, V. Sackmann, H. Stoll, M. Fähnle, T. Tyliszczak, G. Woltersdorf, C. H. Back, and G. Schütz, Phys. Rev. Lett. **101**, 197204 (2008).

[16] M. Curcic, H. Stoll, M. Weigand, V. Sackmann, P. Juellig, M. Kammerer, M. Noske, M. Sproll, B. Van Waeyenberge, A. Vansteenkiste, G. Woltersdorf, T. Tyliszczak, and G. Schütz, Physica Status Solidi B **248**, 2317 (2011).

[17] M. Sproll, M. Noske, H. Bauer, M. Kammerer, A. Gangwar, G. Dieterle, M. Weigand, H. Stoll, G. Woltersdorf, C. H. Back, and G. Schütz, Appl. Phys. Lett. **104**, 012409 (2014).

[18] M. Noske, A. Gangwar, H. Stoll, M. Kammerer, M. Sproll, G. Dieterle, M. Weigand, M. Fähnle, G. Woltersdorf, C. H. Back, and G. Schütz, Phys. Rev. B **90**, 104415 (2014).

[19] D. L. Huber, Phys. Rev. B **26**, 3758 (1982).

[20] L. Berger, J. Appl. Phys. **55**, 1954 (1984).

[21] L. D. Landau and E. M. Lifshitz, Phys. Z. Sowjetunion **8**, 153 (1935).

[22] T. Gilbert, IEEE Trans. Magn. **40**, 3443 (2004).

[23] S. Zhang and Z. Li, Phys. Rev. Lett. **93**, 127204 (2004).

[24] A. Thiaville, Y. Nakatani, J. Miltat, and Y. Suzuki, Europhys. Lett. **69**, 990 (2005).

[25] A. A. Thiele, Phys. Rev. Lett. **30**, 230 (1973).

[26] G. Schütz, W. Wagner, W. Wilhelm, P. Kienle, R. Zeller, R. Frahm, and G. Materlik, Phys. Rev. Lett. **58**, 737 (1987).

[27] K. Y. Guslienko, B. A. Ivanov, V. Novosad, Y. Otani, H. Shima, and K. Fukamichi, J. Appl. Phys. **91**, 8037 (2002).

[28] T. McGuire and R. Potter, IEEE Trans. Magn. **11**, 1018 (1975).

[29] M. Goto, H. Hata, A. Yamaguchi, Y. Nakatani, T. Yamaoka, Y. Nozaki, and H. Miyajima, Phys. Rev. B **84**, 064406 (2011).

[30] R. L. Compton and P. A. Crowell, Phys. Rev. Lett. **97**, 137202 (2006).

[31] A. Vansteenkiste and B. V. de Wiele, J. Magn. Magn. Mater. **323**, 2585 (2011).

[32] J. Sort, K. S. Buchanan, V. Novosad, A. Hoffmann, G. Salazar-Alvarez, A. Bollero, M. D. Baró, B. Dieny, and J. Nogués, Phys. Rev. Lett. **97**, 067201 (2006).

[33] O. G. Heinonen, D. K. Schreiber, and A. K. Petford-Long, Phys. Rev. B **76**, 144407 (2007).

[34] Simulations were carried out for a disk (Py/IrMn) of diameter 1.6 $\mu$m and thickness 30 nm. The antiferromagnet (IrMn) gives rise to an exchange bias coupling, the direction of which was assumed to be parallel (or antiparallel) to the magnetization in the adjacent ferromagnetic (Py) layer. The strength of the exchange bias field is assumed to be 1 mT.